Remote Sensing of Environment 173 (2016) 294–303

Contents lists available at ScienceDirect

Remote Sensing of Environment

journal homepage: www.elsevier.com/locate/rse

# Mapping post-fire habitat characteristics through the fusion of remote sensing tools

Jody C. Vogeler [a,*], Zhiqiang Yang [a], Warren B. Cohen [a,b]

[a] Department of Forest Ecosystems and Society, 321 Richardson Hall, Oregon State University, Corvallis, OR 97331, USA
[b] USDA Forest Service, PNW Research Station, 3200 NW Jefferson Way, Corvallis, OR 97331, USA

ARTICLE INFO

*Article history:*
Received 7 January 2015
Received in revised form 30 July 2015
Accepted 12 August 2015
Available online 21 August 2015

*Keywords:*
Habitat
Landsat time series
Lidar
Maps
Post-fire
Snags
Shrub cover

ABSTRACT

Post-fire snags provide important resources for cavity nesting communities as well as being subject to timber removal through salvage logging practices. Tools that can characterize their distributions along with other features important as wildlife habitat, such as woody shrub cover, would be useful for research and management purposes. Three dimensional lidar data and Landsat time series disturbance products have both shown varying promise in their ability to characterize aspects of dead biomass and understory cover, but studies exploring the combination of the remote sensing datasets calibrated with field data to model difficult to map habitat components are limited. The purpose of this study was to 1) relate lidar and Landsat time series products to field-collected calibration data to produce maps of important post-fire wildlife habitat components including snags of varying sizes and the availability of a woody shrub layer; and 2) compare the individual performance of the Landsat and lidar datasets for predicting the distributions of these difficult to map forest habitat features. Using 164 field calibration plots and remote sensing predictors, we modeled and mapped the distributions of our response variables including snag classes (dbh ≥ 40 cm, ≥50 cm, and ≥75 cm) and woody shrub cover thresholds (≥30 and ≥50% cover) at 10 m resolutions. Remote sensing predictors included various lidar structure and topography variables and Landsat time series products representing the pre-fire forest, disturbance magnitude, and current forest condition. A model was chosen for mapping purposes using AIC model selection and then by comparing leave-one-out-cross-validation error matrices to choose among competing models. We were able to predict and map all response variables with moderate accuracies and variable sensitivity (true positive) and specificity (true negative) rates. All snag and shrub models were considered to have "good" predictive performance as indicated by area under the curve values (0.74–0.91), with percent correctly classified values ranging from 69–85% when a probability threshold is chosen that balances false positive and false negative errors. Landsat models performed marginally better than lidar structure models according to classification statistics. Landsat-only models had slightly less accuracy than models that included lidar and Landsat data, but often with greater errors than the combined model. The ability to map the response variables with moderate errors and acceptable accuracies for many applications was through the fusion of these remote sensing datasets.



## 1. Introduction

Fire patterns are currently in the spotlight due to the concern over deviations from historical fire regimes and potential future climate change impacts (Dale et al., 2001). Fire events and post-fire systems are important in their evolutionary tie with ecosystem functioning and turnover, and wildlife life history strategies (Weber & Flannigan, 1997). They are also of societal interest in areas of human–wildland interface (Radeloff et al., 2005) and in management planning for multiple uses including the natural system, providing timber resources, and minimizing damage to human infrastructures.

Tools that allow for the characterization of these post-fire systems, their distribution across the landscape, and the availability of habitat resources within, would be useful for managers and others interested in the patterns and function of these post-fire areas. Remote sensing has a long history of providing information about wildland fire trends and spatial patterns (Lentile et al., 2006). At the regional and national scales, Landsat satellite imagery provides information about temporal and spatial arrangements of fire events through openly available products such as differenced normalized burn ratio (dnbr) maps, a normalized index of fire severities (Escuin, Navarro, & Fernández, 2008). The 30 m × 30 m spatial and 16 day temporal resolutions of Landsat reflectance data allow for the monitoring of fire events (intensity at time of fire), size (boundaries and year burned), and severity patterns across fire complexes (Lentile et al., 2006). Light detecting and ranging (lidar) is an active remote sensing technology often mounted on an

* Corresponding author.
*E-mail address:* jody.vogeler@oregonstate.edu (J.C. Vogeler).

http://dx.doi.org/10.1016/j.rse.2015.08.011
0034-4257/

airborne platform that can provide predictions of three-dimensional forest structure information (Lefsky, Cohen, Parker, & Harding, 2002). The majority of applications of lidar in post-fire landscapes have involved characterizing fuel loads for fire behavior models (Mutlu, Popescu, Stripling, & Spencer, 2008) and changes in forest structure if pre-and post-fire lidar is available, which is rare (Wulder et al., 2009).

At the local-scale, management of land for multiple purposes requires understanding the three-dimensional aspects of the post-fire landscape and the distribution of specific structural elements such as snags and the availability of a woody shrub component. Post-fire landscapes are important habitats for a variety of wildlife species while also subject to timber removal on many public (Eklund, Wing, & Sessions, 2009) and private lands. More specifically, post-fire snags provide important resources for cavity-nesting communities as foraging, nesting, and roosting substrates (Haggard & Gaines, 2001). Selection of a snag for life history needs may vary by the snag size, species, decay stage, and surrounding landscape properties (Saab, Dudley, & Thompson, 2004). As management activities and changing fire patterns alter the availability and spatial arrangement of snags, there is increasing concern for cavity-nesting communities (Martin & Eadie, 1999). A woody shrub component also influences suitable wildlife habitat by increasing invertebrate abundance, soft mast production, nesting substrates, and concealment from predators (Nappi, Drapeau, & Savard, 2004). Shrub cover is also of interest to timber management as shrubs may compete for resources with regenerating trees (Larson & Franklin, 2005). One particular cavity nesting species of conservation interest associated with these habitat resources is the Lewis's woodpecker, which during the breeding season nests in large snags (often ≥50 cm dbh; Vogeler, 2014) and aerially forages on insects produced in a woody shrub layer (Sousa, 1983). Information about the spatial arrangement of snag classes and woody shrub cover may assist in post-fire research and management efforts for such wildlife species of interest. By providing spatially explicit maps of habitat components, wildlife habitat relationships are then able to be mapped, validated, and improved, a valuable step for management and conservation applications. Although difficult to directly map, studies in unburned forests have found promise in the use of remote sensing data and field-based samples to calibrate models and map the fine scale distribution of snag size classes and woody shrubs (Martinuzzi et al., 2009). To our knowledge, comparable efforts have not been specifically explored in a post-fire landscape where landscape structure and snag dynamics vary.

The purpose of our study was to evaluate the utility of two remote sensing data sets for the prediction and mapping of snags and shrub distributions across a post-fire complex in central Oregon. Our first objective was to relate lidar and Landsat time series products to field-collected calibration data to produce maps of important post-fire wildlife habitat components including snags of varying sizes and the availability of a woody shrub layer. A secondary objective was to compare the individual performance of the Landsat and lidar datasets for predicting the distributions of these difficult to map forest habitat features.

## 2. Methods

### 2.1. Study area

Our study was conducted in the B&B Fire Complex within the Deschutes National Forest located in the Cascade Mountains of central Oregon (Fig. 1). The fire complex was created when two fires, the Bear Butte Fire and the Booth Fire that ignited on the same day in the summer of 2003, burned together to cover 36,732 ha (90, 769 acres) with a mosaic of fire severities. Our study area is constrained to coinciding lidar coverage within the fire perimeter that covers about a 28,000 ha area which includes the majority of the fire complex on the east side of the Pacific Crest. Elevations ranged from 822–2182 m, with higher

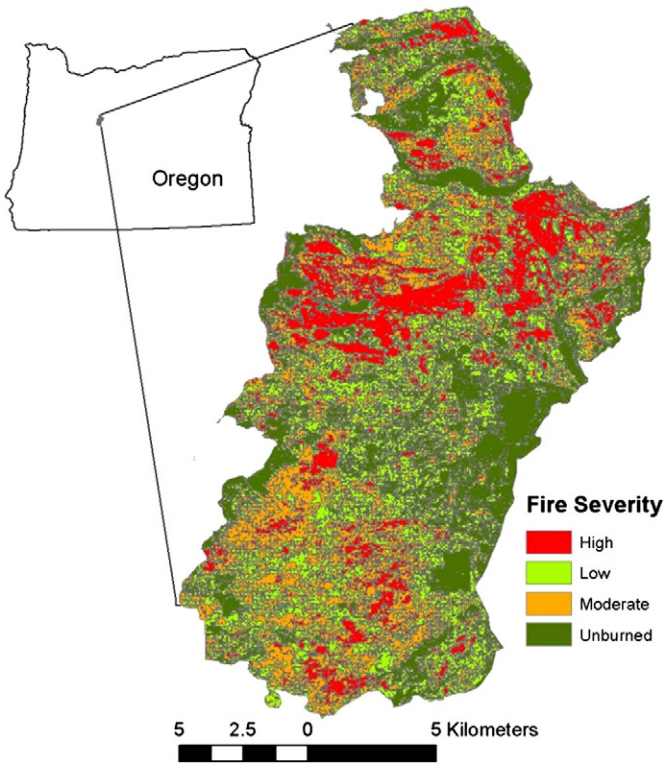


**Fig. 1.** B&B fire complex (2003) located within central Oregon and the mosaic of fire severities represented by the previously mapped differenced normalized burn ratio for the area of overlap between the fire complex and coinciding lidar coverage.

elevations occurring within the Mount Jefferson Wilderness Area. The mixed conifer forest was dominated by the wet and dry varieties of several previous mapped plant association groups (PAG): ponderosa pine (*Pinus ponderosa*), mixed-conifer, lodgepole pine (*Pinus contorta*), and mountain hemlock (*Tsuga mertensiana*). The most frequently observed shrub genus within our field surveys were Ceanothus (*Ceanothus sp*), willow (*Salix sp.*), and manzanita (*Arctostaphylos sp.*).

### 2.2. Identifying important habitat components

We defined snags for the purpose of our project as standing dead trees. To identify important snag size classes utilized by the cavity nesting community within the B&B Fire Complex, we conducted cavity nest surveys for 18 avian species of primary cavity excavators (species that create cavities), weak cavity excavators (may utilize pre-existing cavities or excavate when suitable snags are available and/or cavity resources are limited), and secondary cavity users (utilize pre-existing cavities) during the 2012 breeding season. We monitored nests every 3–6 days until fledge or fail. Following the breeding season, we measured nest trees (n = 148) and determined thresholds that represent snag size classes utilized in greater proportions than their availability on the landscape as determined from random sample plots (Table 1).

**Table 1**
Use of snags at varying size thresholds by cavity nesters in the B&B Fire Complex compared to the availability of snag classes as sampled in field plots (Available). Cavity nesting groups include primary cavity excavators (PCEs), weak cavity excavators (WCEs), and secondary cavity users (SCUs).

| Percent use/availability of snags | | | | | |
|---|---|---|---|---|---|
| Snag class | All nests | PCEs | SCUs | WCEs | Available |
| dbh ≥ 40 cm | 77.6 | 96.6 | 70.0 | 42.9 | 21.9 |
| dbh ≥ 50 cm | 55.9 | 70.7 | 48.8 | 42.9 | 10.4 |
| dbh ≥ 75 cm | 19.6 | 17.2 | 20.0 | 28.6 | 2.3 |

We identified three snag size classes to include in our modeling efforts: snags with a diameter at breast height (dbh) ≥40 cm, ≥50 cm, and ≥75 cm (Table 1). We also selected two shrub cover thresholds representing moderate (≥30%) and high (≥50%) shrub cover. From here on out we will refer to this combined set of snag and shrub metrics as our response variables.

### 2.3. Field vegetation data collection

Vegetation data was collected at 164 15-meter (m) radius field sample plots (here by referred to as plots) during the summers of 2012 and 2013. Plots were stratified by the dominant PAG and fire severity to attempt to capture the variability of post-fire stands. We collapsed the PAG polygons down to three main forest types for a simpler stratification: ponderosa pine, mixed-conifer, and an alpine category that included the higher elevation lodgepole pine and mountain hemlock zones. A previously created Landsat fire severity dataset provided through the Monitoring Trends in Burn Severity program (MTBS; Eidenshink et al., 2007) was used for the purpose of stratification using the classes of unburned, low, moderate, and high severities. We used a Trimble GeoExplorer GPS unit to record the location of plot centers. A minimum of 150 logged points were collected by the GPS and later differentially corrected using online base station files resulting in a horizontal accuracy of <1 m for the majority of our plot locations. All trees ≥12 cm dbh within a 15 m radius of plot center were included in data collection. One crew member recorded all measurements while stem mapping trees from plot center using an Impulse Laser Rangefinder for distance and a compass for bearings, while a second crew member collected attree measurements. For all trees we measured height (using rangefinder), dbh, decay stage, top condition (broken top vs. intact), percent remaining bark, species if identifiable, and number of cavities present. We used a designation of 0 (live) to 5 (severely burnt and misshapen with spongy wood) decay stage for the snags, with the middle stages associated with the proportion of primary (large) and secondary (fine) branches remaining and the snag top condition. Stem-mapping the field plots allowed flexibility in the scale at which to summarize the snag variables for applicability in multiple projects. For the purpose of this study, we summarized metrics within a 5.64 m radius from plot center to represent the fine-scale variability in the distributions of focal snag variables. Comparable to this scale, we created 5 m radius center subplots, where we collected maximum shrub height and ocular estimations for shrub cover, ground cover characteristics, and seedling/sapling counts by species for each subplot quadrant, which we later averaged. From this average shrub cover estimation, we designated presence or absence of shrub cover for modeling purposes using 30% and 50% cover thresholds representing the availability of moderate and high woody shrub cover.

### 2.4. Lidar acquisition and processing

Lidar data was provided as part of a larger Deschutes National Forest data acquisition by Watershed Sciences flown between 2009 and 2010 depending on area of interest. The northwest portion of our study area was flown on July 25, 2010 with the remaining area covered in October 2009 flights. The Leica ALS50 Phase II and ALS60 sensors had a pulse rate of >105 kHz, average pulse density of 8.6/m$^2$, and an average accuracy of 0.04 m. Plot and grid lidar metrics were processed within FUSION (McGaughey, 2009). We used cylinders representing plot radii to clip the lidar data and calculate height, density, and intensity cloud metrics. Gridmetrics allowed us to calculate corresponding 10 × 10 m rasters, representing the same spatial area as our 5.64 m radius circular plots. Height and density metrics were summarized using lidar returns above 1 m, and canopy cover with returns over 2 m (Table 2). We clipped the lidar grids by the B & B Fire boundary and filled in no-data cells with zero values using a constant mask raster matching the lidar grids in ArcGIS 10.1. These no-data cells were a product of lower height thresholds in the lidar processing and thus represent areas without vegetation cover above these thresholds. Also in ArcGIS, we aggregated 1 m lidar Bare Earth grid rasters delivered by Watershed Sciences to 10 m grids of elevation, percent and degree slope, and aspect. From these grids, we produced frequently used aspect transformations within raster calculator (Table 2).

### 2.5. Landsat processing

In the processing of Landsat time series images, we used a cloud mask to make an annual composite for all years leading up to, and following the fire event. We calculated tasseled-cap brightness, greenness, and wetness metrics for all yearly composite images (Crist, 1985). For the remainder of the analyses, we chose to focus on only a few of the possible Landsat time-series products (see Pflugmacher, Cohen, Kennedy, & Yang, 2014 for additional time-series metrics). Our focal metrics included: the year prior to the fire (2002) to represent pre-fire condition; the change in tasseled-cap values from the pre-fire condition to the year following the fire event (due to the timing of the fire, the disturbance was either detected as 2003 or 2004); and the tasseled-cap values from the 2010 composite image to coincide with lidar data collection and represent current conditions. We used the change in tasseled-cap pre- and post-disturbance to represent continuous measures of vegetation change as a result of the fire event. The goal of this study was to create predictive maps of the response variables at a

**Table 2**
Model metric descriptions and abbreviations including the response habitat metrics summarized from 5.64 m radius field plots and the groups of remote sensing predictor datasets included in models.

| Model metric descriptions | |
|---|---|
| *Presence/absence response variables* | |
| Snag ≥ 40 cm | Snags ≥ 40 cm dbh |
| Snag ≥ 50 cm | Snags ≥ 50 cm dbh |
| Snag ≥ 75 cm | Snags ≥ 75 cm dbh |
| Shrub30% | Woody shrub cover ≥ 30% |
| Shrub50% | Woody shrub cover ≥ 50% |
| *Landsat predictor variables* | |
| TCG_PRE | Tasseled cap greenness value the year prior to fire even |
| TCW_PRE | Tasseled cap wetness value the year prior to fire even |
| TCG_CHANGE | Change in tasseled cap greenness values before and after fire event |
| TCW_CHANGE | Change in tasseled cap wetness values before and after fire event |
| TCG_2010 | Tasseled cap greenness value from 2010 yearly composite |
| TCW_2010 | Tasseled cap wetness value from 2010 yearly composite |
| *Lidar structure and intensity predictor variables* | |
| COVER | Percent canopy cover above 2 m |
| HTMEAN | Mean height of lidar vegetation returns above 1 m |
| HTSTD | Standard deviation of heights for lidar returns above 1 m |
| HTCV | Coefficient of variation of height of returns above 1 m |
| CRR | Canopy relief ratio = (mean height-minimum height)/(max height-minimum height) |
| INTMEAN | Mean of lidar return intensity |
| INTSTD | Standard deviation of lidar return intensities |
| STRAT2 | Stratum 2 = proportion of lidar returns between 1 and 2.5 m aboveground |
| STRAT3 | Stratum 3 = proportion of lidar returns between 2.5 and 10 m aboveground |
| STRAT4 | Stratum 4 = proportion of lidar returns between 10 and 20 m aboveground |
| STRAT5 | Stratum 5 = proportion of lidar returns between 20 and 30 m aboveground |
| STRAT6 | Stratum 6 = proportion of lidar returns between 30 and 40 m aboveground |
| STRAT7 | Stratum 7 = proportion of lidar returns >40 m aboveground |
| *Lidar topography predictor variables* | |
| ELEV | Lidar derived elevation |
| SLOPE | Lidar derived degree slope |
| ASPECT | Transformed lidar derive Aspect = COS*[45-Aspect(degrees)] + 1 |
| SSINA | Percent slope * SIN * Aspect (degrees) |
| SCOSA | Percent slope * COS * Aspect (degrees) |

**Table 3**
Model statistics for models with the lowest AIC values for each habitat response metric and remote sensing predictor set. Combined models incorporate both lidar and Landsat metrics. Models in bold represent competing models following AIC model selection when comparing predictor sets and combined models. Indicators for varying levels of significance for parameters include: *** <0.001, ** <0.01, * <0.05,. <0.1.

| Presence/absence response | | Best model variables | AIC | AUC |
|---|---|---|---|---|
| Snag 40 cm | **Combined** | **TCW_PRE (*), TCG_2010 (***), TCW_2010 (***), HTSTD (.)** | **178.43** | **0.77** |
| | **Landsat** | **TCW_PRE (**), TCG_2010 (***), TCW_2010 (***)** | **180.06** | **0.73** |
| | Lidar structure | COVER (**), HTSTD (*), STRAT7 | 193.03 | 0.64 |
| | Lidar topography | Intercept only | 202.02 | 0.55 |
| Snag 50 cm | **Combined** | **TCW_PRE (.), TCG_2010 (***), TCW_2010 (***), STRAT5 (.)** | **209.09** | **0.74** |
| | **Landsat** | **TCW_PRE (*), TCG_2010 (***), TCW_2010 (***)** | **210.03** | **0.72** |
| | Lidar structure | COVER (***), HTMEAN (*), STRAT2, STRAT5 (.) | 221.92 | 0.69 |
| | Lidar topography | ELEV (*) | 226.82 | 0.50 |
| Snag 75 cm | **Combined** | **TCG_CHANGE (.), TCG_2010 (***), TCW_2010 (***), CRR (*), INTSTD (,), STRAT2, STRAT5 (*), STRAT7, ELEV (**)** | **93.12** | **0.90** |
| | Landsat | TCG_PRE (.), TCG_CHANGE (*), TCG_2010 (*), TCW_2010 (*) | 112.87 | 0.80 |
| | Lidar structure | COVER (**), HTMEAN (*), INTMEAN (.), STRAT2 (*), STRAT5 (*), STRAT7 | 118.34 | 0.77 |
| | Lidar topography | ELEV (**), SLOPE | 120.18 | 0.68 |
| Shrub 30% | **Combined** | **TCG_PRE (***), TCG_CHANGE (***), TCG_2010 (***), HTMEAN (*), HTCV (.), STRAT5 (*), ELEV (**), SLOPE (.)** | **131.02** | **0.90** |
| | Landsat | TCG_PRE (**), TCG_CHANGE (***), TCG_2010 (***) | 140.39 | 0.87 |
| | Lidar structure | COVER (***), HTCV, INTSTD (**), STRAT5 (*) | 172.64 | 0.78 |
| | Lidar topography | ELEV (***), SLOPE (***) | 190.53 | 0.69 |
| Shrub 50% | **Combined** | **TCG_PRE (***), TCG_CHANGE (***), TCG_2010 (***), HTCV, ELEV (*), SLOPE (*), SSINA (.)** | **114.26** | **0.91** |
| | Landsat | TCG_PRE (**), TCG_CHANGE (***), TCG_2010 (***) | 119.12 | 0.89 |
| | Lidar structure | COVER (***), HTCV (*), INTSTD (*), STRAT5 | 159.97 | 0.77 |
| | Lidar topography | ELEV (**), SLOPE (***) | 170.91 | 0.70 |

fine resolution providing flexibility in applications, the ability to represent local-scale variability, and to facilitate opportunities to create density measures of the snag classes by aggregating to project-specific scales (Vogeler, 2014). Initial explorations into the field-collected plot data identified 10 m grids (and associated 5.64 m radius plots) as a focal scale where snags at the dbh thresholds were only found in small numbers (range 0–5, although majority were between 0–2 for a single 5.64 m radius plot), and at which the dataset reflects relatively well balanced presence and absence ratios for logistic regression analyses. This resolution also closely matches that of the field-collected shrub data. We resampled the Landsat grids to match the 10 m lidar grids.

### 2.6. Statistical models

Zonal statistics within ArcGIS 10.1 were used to extract Landsat summary metrics for the plot areas using a 5.64 m radius buffer around field plot centers. The average values of Landsat predictor metrics within the buffers from the zonal statistics tables were used from this point forward in statistical analyses. Lidar metrics were provided at this scale during the cloudmetrics step described above. Highly correlated variables were removed using a variance inflation factor (VIF) threshold of <10, although the majority of VIF values were <3. This resulted in the exclusion of some lidar structure variables and all tasseled-cap brightness values, but retained all greenness and wetness metrics and a variety of lidar height, density, cover, intensity, and topography metrics (see Table 2 for descriptions and abbreviations). We used logistic regression with a binomial error distribution to model the relationship between the response variables and the Landsat and lidar vegetation and topography metrics. Our modeling approach assumes a logit link function which is defined in the following model:

$$\text{logit}(\theta) = \ln(\theta_i/(1\text{-}\theta_i) = \beta_0 + \beta_1 X_{i1} + \beta_2 X_{i2} + \cdots + \beta_U X_{iU} + e_i \quad ;$$

where θ is the probability of occurrence for the *i*th sampling unit, x's are the predictor variable values measured at that sampling unit, the β's are the coefficients for the parameters, where $\beta_0$ is the intercept term, and e indicates residual uncertainty (MacKenzie, 2006). The coefficients were estimated using maximum likelihood techniques (Agresti, 2007). Probability of occurrence output from logistic regression have values ranging from 0, denoting no probability of occurrence, to 1.0, representing the greatest probability of occurrence. The threshold chosen to predict a presence or absence impacts the accuracy and associated error structure and can be adjusted to cater to different project objectives and priorities. When comparing two possible methods for predicting the binary

**Table 4**
Error and accuracy rates for snag and shrub classifications comparing three options for assigning presence/absence thresholds to the probability of occurrence output. The default threshold remains fixed at 0.5, others are model specific including the threshold where false positive and false negative error rates are balanced (FPR = FNR), and the threshold at which the percent correctly classified is maximized (MaxPCC). Also reported are model sensitivity (Sens) and specificity (Spec) rates.

| Response | Method | Threshold | PCC | Sens | Spec | FPR | FNR |
|---|---|---|---|---|---|---|---|
| Snag ≥ 40 cm | Default | 0.50 | 76 | 0.92 | 0.37 | 0.63 | 0.08 |
| | FPR = FNR | 0.71 | 69 | 0.69 | 0.69 | 0.31 | 0.31 |
| | MaxPCC | 0.43 | 78 | 0.97 | 0.35 | 0.65 | 0.03 |
| Snag ≥ 50 cm | Default | 0.50 | 67 | 0.65 | 0.69 | 0.31 | 0.35 |
| | FPR = FNR | 0.49 | 67 | 0.68 | 0.66 | 0.34 | 0.32 |
| | MaxPCC | 0.43 | 71 | 0.85 | 0.58 | 0.42 | 0.15 |
| Snag ≥ 75 cm | Default | 0.50 | 85 | 0.52 | 0.94 | 0.06 | 0.48 |
| | FPR = FNR | 0.29 | 81 | 0.81 | 0.81 | 0.19 | 0.19 |
| | MaxPCC | 0.52 | 85 | 0.52 | 0.94 | 0.06 | 0.48 |
| Shrub30% | Default | 0.50 | 82 | 0.63 | 0.90 | 0.10 | 0.37 |
| | FPR = FNR | 0.34 | 84 | 0.85 | 0.84 | 0.16 | 0.15 |
| | MaxPCC | 0.61 | 85 | 0.60 | 0.96 | 0.04 | 0.40 |
| Shrub50% | Default | 0.50 | 90 | 0.70 | 0.97 | 0.03 | 0.30 |
| | FPR = FNR | 0.29 | 85 | 0.85 | 0.85 | 0.15 | 0.15 |
| | MaxPCC | 0.50 | 90 | 0.70 | 0.97 | 0.03 | 0.30 |

**Table 5**
Combined model results for each habitat metric Results include parameter estimates and 95% confidence intervals (CI lower, CI upper). Indicators for varying levels of significance for parameters include: *** <0.001, ** <0.01, * <0.05,. <0.1.

| Response | Parameter | Estimate | Std. Error | CI lower | CI upper | z-value | sig |
|---|---|---|---|---|---|---|---|
| Snag ≥ 40 cm | (Intercept) | −6.778 | 1.730 | −10.395 | −3.564 | −3.940 | *** |
| | TCW_PRE | 0.001 | 0.001 | 0.000 | 0.003 | 2.604 | ** |
| | TCG_2010 | 0.003 | 0.001 | 0.002 | 0.004 | 4.476 | *** |
| | TCW_2010 | −0.004 | 0.001 | −0.006 | −0.002 | −4.419 | *** |
| | HTSTD | 0.137 | 0.080 | −0.017 | 0.300 | 1.863 | . |
| Snag ≥ 50 cm | (Intercept) | −7.092 | 1.783 | −10.847 | −3.818 | −3.977 | *** |
| | TCW_PRE | 0.001 | 0.001 | 0.000 | 0.002 | 1.916 | . |
| | TCG_2010 | 0.003 | 0.001 | 0.002 | 0.004 | 4.634 | *** |
| | TCW_2010 | −0.003 | 0.001 | −0.005 | −0.002 | −3.635 | *** |
| | STRAT5 | 0.048 | 0.029 | −0.007 | 0.109 | 1.663 | . |
| Snag ≥ 75 cm | (Intercept) | −18.750 | 5.735 | −31.402 | −8.564 | −3.269 | ** |
| | TCG_CHANGE | 0.001 | 0.001 | 0.000 | 0.003 | 1.739 | . |
| | TCG_2010 | 0.008 | 0.002 | 0.004 | 0.012 | 3.728 | *** |
| | TCW_2010 | −0.011 | 0.003 | −0.019 | −0.006 | −3.557 | *** |
| | CRR | 3.562 | 1.815 | 0.264 | 7.470 | 1.963 | * |
| | INTSTD | 0.061 | 0.032 | 0.003 | 0.130 | 1.932 | . |
| | STRAT2 | 0.150 | 0.114 | −0.054 | 0.429 | 1.322 | |
| | STRAT5 | 0.124 | 0.052 | 0.028 | 0.237 | 2.374 | * |
| | STRAT7 | 0.908 | 0.925 | −0.175 | 3.647 | 0.982 | |
| | ELEV | −0.011 | 0.004 | −0.019 | −0.005 | −2.914 | ** |
| Shrub 30% | (Intercept) | 2.082 | 2.316 | −2.401 | 6.766 | 0.899 | |
| | TCG_PRE | −0.006 | 0.002 | −0.009 | −0.003 | −3.537 | *** |
| | TCG_CHANGE | −0.004 | 0.001 | −0.007 | −0.003 | −4.509 | *** |
| | TCG_2010 | 0.005 | 0.001 | 0.003 | 0.007 | 5.215 | *** |
| | HTMEAN | −0.107 | 0.043 | −0.195 | −0.027 | −2.500 | * |
| | HTCV | 5.199 | 2.870 | −0.262 | 11.085 | 1.812 | . |
| | STRAT5 | 0.089 | 0.038 | 0.012 | 0.168 | 2.324 | * |
| | ELEV | −0.005 | 0.002 | −0.009 | −0.001 | −2.667 | ** |
| | SLOPE | 0.124 | 0.074 | −0.018 | 0.280 | 1.665 | . |
| Shrub 50% | (Intercept) | 0.903 | 2.448 | −3.914 | 5.774 | 0.369 | |
| | TCG_PRE | −0.007 | 0.002 | −0.010 | −0.003 | −3.662 | *** |
| | TCG_CHANGE | −0.004 | 0.001 | −0.006 | −0.003 | −4.494 | *** |
| | TCG_2010 | 0.006 | 0.001 | 0.004 | 0.008 | 5.096 | *** |
| | HTCV | 4.514 | 2.861 | −0.898 | 10.387 | 1.578 | |
| | ELEV | −0.005 | 0.002 | −0.009 | −0.001 | −2.548 | * |
| | SLOPE | 0.160 | 0.075 | 0.014 | 0.313 | 2.137 | * |
| | SSINA | 0.052 | 0.029 | −0.004 | 0.110 | 1.805 | . |

response of the occurrence of snags, Eskelson, Temesgen, and Hagar (2012) found better predictive performance and flexibility in threshold selection procedures using logistic regression as opposed to another frequently used method in forest attribute modeling, nonparametric random forest nearest neighbor imputation technique. The generalized linear models (GLMs) were created in R (R Development Core Team, 2014) and competing models were selected using an AIC model selection approach (Burnham & Anderson, 2002).

To compare predictive performance and to evaluate any model improvements by using the combination of remote sensing metrics, model runs were conducted for each response variable using the combined predictor set, a Landsat-only set, a lidar structure-only set, and a lidar-estimated topography set. Accuracy and error values were calculated using leave-one-out-cross-validation (loocv) prediction values. For the model with the smallest AIC value for each response variable, we created confusion matrices and associated statistics including: percent correctly classified (PCC), false positive rate (FPR), and false negative rate (FNR). We assessed false negative (omission) and false positive (commission) error rates using three of the possible methods for selecting an optimal threshold at which to assign presence/absence predictions to the probability of occurrence model outputs: default 0.5; threshold at which sensitivity (true positive rate) and specificity (true negative rate) are balanced; and where PCC is maximized. Project goals determine the level and type of error appropriate and thus which threshold will best meet that purpose. Receiver operator curves (ROC) were created for the selected model for each response variable and predictor set. We calculated area under the curve (AUC) values as a way to evaluate predictive performance regardless of the probability of occurrence threshold chosen (Guisan & Zimmermann, 2000). AUC values can range between 0.5 depicting no model discrimination to 1.0 representing perfect model performance. We followed the interpretations presented by Pearce and Ferrier (2000) where AUCs between 0.7–0.9 represent reasonably good model discrimination appropriate for most purposes, and AUCs >0.9 reflecting excellent model

**Table 6**
Parameters and associated significance for the selected combined model for each habitat response variable. Indicators for varying levels of significance for parameters include: *** <0.001, ** <0.01, * <0.05,. <0.1, ns = not significant but included in the model.

| Response | Predictors | | | | | | | | | | | |
|---|---|---|---|---|---|---|---|---|---|---|---|---|
| | (Intercept) | TCG_PRE | TCW_PRE | TCG_CHANGE | TCW_CHANGE | TCG_2010 | TCW_2010 | COVER | HTMEAN | HTSTD | HTCV | CRR |
| Snag ≥ 40 cm | *** | | ** | | | *** | *** | | | | | |
| Snag ≥ 50 cm | *** | | | | | *** | *** | | | | | |
| Snag ≥ 75 cm | ** | | | | | *** | *** | | | | | * |
| Shrub 30% | ns | *** | | *** | | *** | | | * | | | |
| Shrub 50% | ns | *** | | *** | | *** | | | | | ns | |

performance. Accuracy measures from logistic regression may be inflated by highly unbalanced presence/absence datasets (Agresti, 2007; Freeman & Moisen, 2008; McPherson, Jetz, & Rogers, 2004). Due to a large number of absence plots for the snag class dbh ≥ 75 cm, we took a random subset the absences using the regsubsets function in R (Lumley, 2013), to reach a minimum balance ratio of 0.3 between presence and absence (Ruiz-Gazen & Villa, 2008).

### 2.7. Predictive mapping

The rgdal package in R was used to apply selected models to the 10 m predictor grids to create probability of occurrence maps for each of the response variables. We chose the threshold for probability of occurrence where sensitivity and specificity were balanced to map presence/absence, although perhaps the more valuable products are the probability of occurrence maps which allow the users to define the threshold that best meets their project priorities which may vary from our own.

## 3. Results

We were able to predict the distribution of snags and shrubs in a post-fire landscape using remote sensing and field-collected calibration data with acceptable overall predictive performance (Table 3) according to AUC values (Pearce & Ferrier, 2000), and variable sensitivity and specificity rates. The moderate and high shrub cover metrics had the greatest percent correctly classified rates (84% and 85%, respectively) and the smallest error rates (0.15–0.16 for FPRs and FNRs where specificity and sensitivity were balanced; Table 4). Among the snag classes, map accuracies were the greatest for the largest snag class, with PCC rates between 67% and 81% and error rates ranging from 0.19–0.34 for the snag size classes (Table 4). When viewing the map classification performance at the probability of occurrence threshold which maximizes the PCC rate, shrub maps exhibited better specificity than sensitivity and snag classification performances varied by size class (Table 4).

Within the combined model runs including Landsat and lidar metrics, Landsat tasseled-cap metrics from 2010 were found in models that produced greatest map accuracies for all response variables (Table 5). We considered model metrics significant at a 95% confidence level when coefficient confidence intervals did not include zero. TCG_2010 displayed a significant positive relationship with all response variables (parameter estimate significantly >0), while TCW_2010 had significant negative influences on the presence of all snag size classes (parameter estimate significantly <0; Table 5). Pre-fire Landsat tasseled-cap metrics were included in several selected models. TCG_PRE negatively influenced both shrub cover metrics, while TCW_PRE was positively related to the occurrence of snags with dbh ≥ 40 cm (Table 5). The disturbance change in tasseled-cap metrics was only significant for Shrub 30% and Shrub 50%, where there were negative relationships with TCG_CHANGE (Table 5).

The only lidar structure metric that was included in the selected combined model for more than one snag or shrub variable was STRAT5 (20–30 m stratum) although only providing a significant improvement to the quality of model fit for the largest dbh snag class and moderate shrub cover (Table 6). As the proportion of lidar returns increased in STRAT5, so did the probability of occurrence of snags dbh ≥ 75 cm and shrub cover ≥ 30% (Table 5). That is not to say that there were not multiple significant relationships between lidar structure metrics and the response variables in the lidar only runs, but these relationships were masked by the importance of the time series metrics in the combined models for driving map classifications (Table 3). Elevation was a significant predictor in selected models for snags ≥ 75 cm and both shrub classes (Table 6), where the probability of occurrence for snags dbh ≥ 75 cm and the shrub cover classes decreased as elevation increased (Table 5).

When categories of predictor variables were separated into individual model runs, Landsat-only maps performed marginally better than lidar structure map classifications for all response variables (Table 3). For snags with dbh ≥ 40 cm and dbh ≥ 50 cm, the selected Landsat-only model was even competitive with the combined run following AIC model selection where models with ΔAIC < 2 are considered competitive (Table 3). The topography predictor set had the least predictive strength for all response variables according to map accuracies, although there were fewer topography metrics than in the other model sets (Table 1). In the lidar structure-only model runs, COVER was a significant negative predictor in all selected models (Table 3).

Spatially continuous Landsat and lidar predictor variables allowed us to map predicted relationships within the selected models for the snag (Fig. 2) and shrub (Fig. 3) habitat metrics across the post-fire landscape. We found that the threshold chosen to predict presence and absence had varying impacts on the false negative and false positive prediction errors and overall accuracies depending on the response variable (Table 2).

## 4. Discussion

The combination of passive Landsat reflectance data through time along with current fine-scale structure and topographic data provided by lidar allowed us to map important habitat components including the predicted probability of occurrence of snag size classes and woody shrubs across a post-fire landscape with moderate map accuracies and variable errors. Although Landsat time series models outperformed lidar structure models following AIC model selection when compared independently, Landsat-only predictive maps often exhibited larger classification error rates than maps that combined the two remote sensing data sets. Our results add to a growing body of literature finding value in the combination of multiple remote sensing datasets and corresponding field data for modeling forest systems (Dalponte, 2008; Goetz et al., 2010; Hudak et al., 2006), although few studies have explored this utility to map fine-scale post-fire structure components (Bishop, Dietterick, White, & Mastin, 2014; Wulder et al., 2009).

While lidar has become an attractive option for mapping structural habitat components, recent improvements in extracting the full value of Landsat stacks are advancing the mapping of forest systems appropriate for wildlife habitat purposes as well. Spectral information about pre-disturbance forest in conjunction with magnitude of change and current spectral properties were important predictors for many of the response variables in this study. Characteristics of pre-disturbance forest

| INTMEAN | INTSTD | STRAT2 | STRAT3 | STRAT4 | STRAT5 | STRAT6 | STRAT7 | ELEV | SLOPE | ASPECT | SSINA | SCOSA |
|---|---|---|---|---|---|---|---|---|---|---|---|---|
| | | ns | | | * | | ns | ** | | | | |
| | | | | | * | | | ** | | | | |
| | | | | | | | | * | * | | | |

condition can help predict what remains following the disturbance event, especially when paired with information about the magnitude of change (Pflugmacher, Cohen, & Kennedy, 2012). When considering the occurrence of large snags following a fire, there must first have been mature enough pre-fire forest conditions to contain large trees (Nappi & Drapeau, 2011). Variations in the magnitude of change may help us predict crown mortality, and thus the chance of standing dead trees following the fire event (Nappi & Drapeau, 2011). Pflugmacher et al. (2012) examined the importance of disturbance and recovery information from Landsat time series for predicting current forest structure conditions compared to lidar and single-date Landsat imagery. Of note, the study found time series disturbance and recovery metrics were better predictors of aboveground dead biomass than current lidar structure data (Pflugmacher et al., 2012), which corresponds to our findings as to the importance of the time series metrics for modeling our snag classes. Utilizing time series methods also provides the opportunity for long term monitoring of forest conditions and changes in wildlife habitat (Davis, Dugger, Mohoric, Evers, & Aney, 2011).

While our study found Landsat time series metrics as important drivers of post-fire snag and shrub distributions, lidar structure and topography metrics also contributed to the predictive capabilities of the selected combined models. Few studies have attempted to map snag distributions at fine-scales in a post-fire forest system using remote sensing (Wing, Eklund, & Sessions, 2010; Wing, Ritchie, Boston, Cohen, & Olsen, 2015). Wing et al. (2010) manually located trees within lidar point clouds in a post-fire landscape by focusing in on known tree locations. The study found good support for the ability of lidar to accurately locate trees and extract heights as well as condition (live vs. dead) although these efforts were restricted to localized plots and not mapped across the landscape (Wing et al., 2010). Wing et al. (2015) used a multistep lidar point cloud filtering approach to identify snags in burned and unburned study areas in northeastern California with moderate success. The study had an overall snag detection rate of 58.5% (±3.7%) using a computer intensive technique that could prove difficult for many projects to replicate. In comparison, our study utilized widely available FUSION lidar metrics and Landsat products and provided information about snag size classes, an important criteria for assessing habitat suitability for many species, with overall snag prediction accuracies of ≥67%. Our largest snag class exhibited the best classification accuracies while also the only highly imbalanced data set for which we randomly subset the absences. While our target balance ratio of 0.3 was more conservative than suggested by previous studies (Ruiz-Gazen & Villa, 2008), we acknowledge that the results are dependent on the particular sample of absence plots randomly selected. Although also an important structure component of forest systems for wildlife habitat needs, directly mapping woody shrub distributions using remote sensing, even with three-dimensional lidar data, can be difficult in areas of high canopy cover and where the understory is made up of other non-shrub components (Martinuzzi et al., 2009). In our 9 or 10 year post-fire study area, there was large amounts of down wood and coniferous re-growth complicating the extraction of shrub information from lidar point cloud data, but our results show promise in our model's ability to pick out shrubs from these other components (overall accuracy of 84% and 85% for moderate- and high-shrub cover, respectively). These shrub model

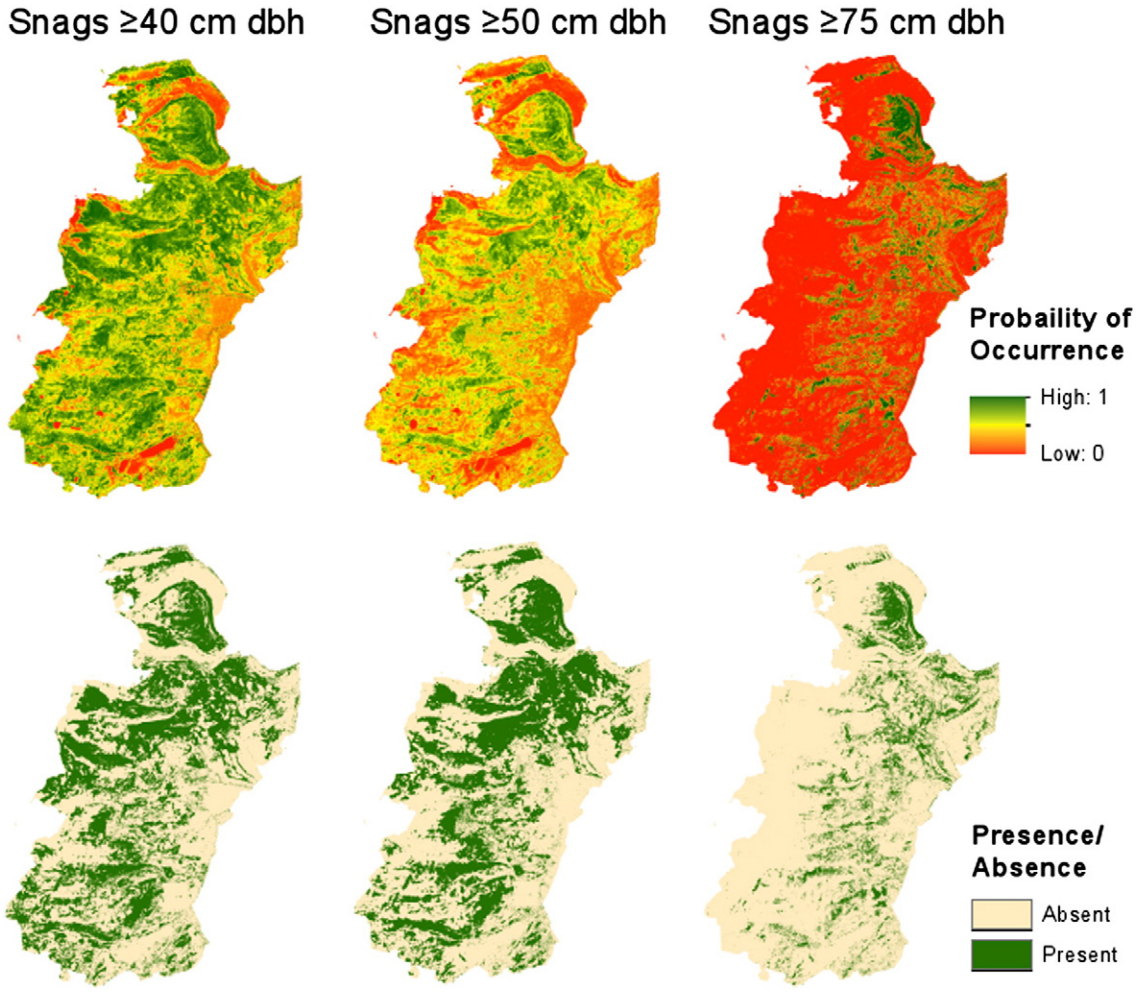


**Fig. 2.** Probability of occurrence maps for snag size classes. Presence/absence mapped using the probability threshold where sensitivity and specificity are balanced (Snag ≥ 40 cm = 0.71; Snag ≥ 50 cm; Snag ≥ 75 cm).

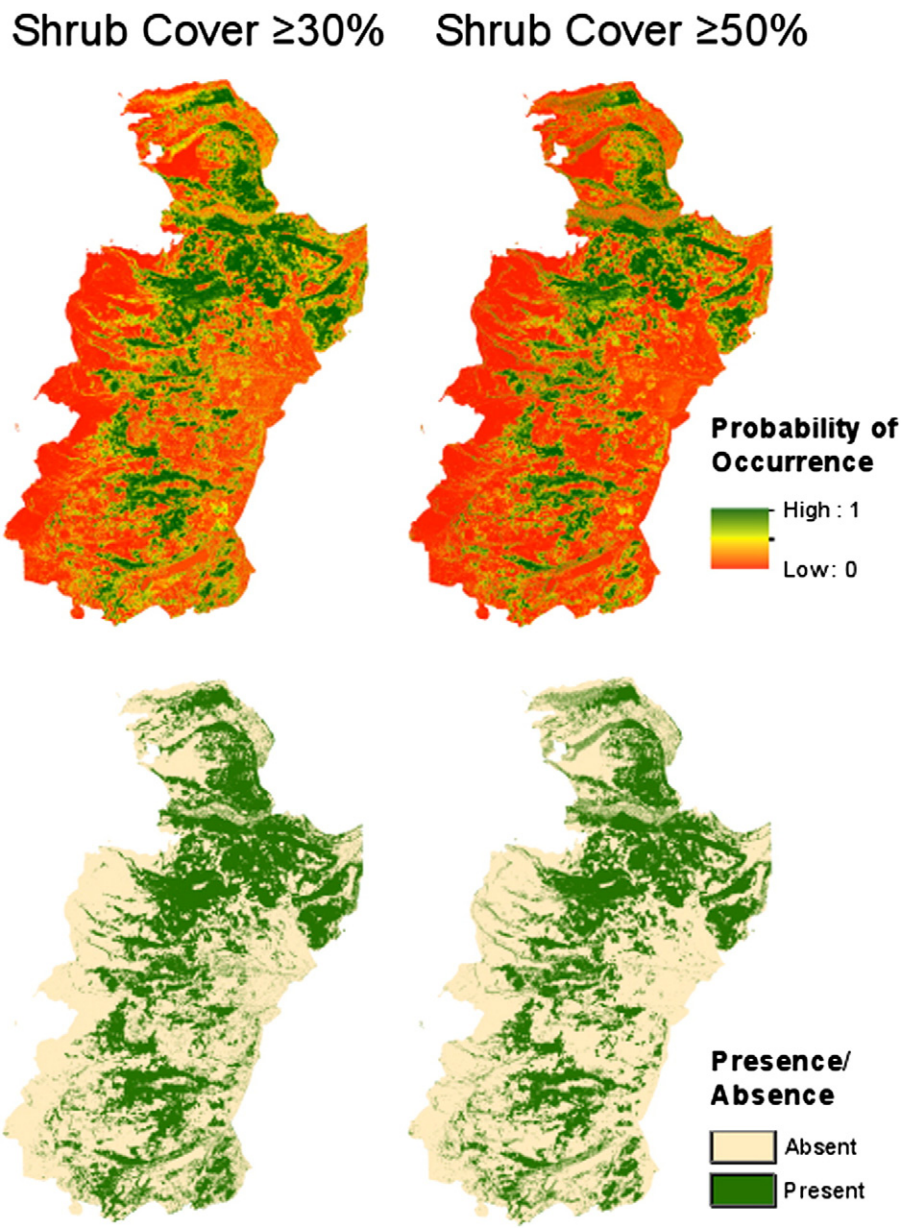


**Fig. 3.** Probability of occurrence maps for shrub cover classes, including moderate- (≥30%) and high-shrub cover (≥50%). Presence/absence mapped using the probability threshold where sensitivity and specificity are balanced (moderate cover = 0.34; high cover = 0.29).

accuracies are comparable to Martinuzzi et al. (2009) in their unburned study area where they used a threshold of ≥25% shrub cover with an overall prediction accuracy of 83%.

Lidar data is limited in spatial and temporal coverage and comes at a cost to projects; therefore there is value in being able to extract spatially continuous habitat components and change through time using Landsat products. Ideally, the temporal and spatial availability of lidar datasets will improve so that we can utilize the full range of existing remote sensing technology including important structural information from lidar, in creating the best habitat monitoring and management products possible. The rich structure data, acquisition costs, and required processing skillsets lead to the utilization of lidar datasets for years following the actual year of collection (Vierling, Swift, Hudak, Vogeler, & Vierling, 2014). In our study there was a 2–4 year time lag between lidar acquisition and field surveys depending on the particular sample plot and which flight covered that location. While all salvage logging had been completed prior to this time, snag fell rates increase with time since fire (Everett et al., 2000), and thus could add to prediction errors in relating lidar structure data with field collected metrics. The Fire and Fuel Extension to the Forest Vegetation Simulator for our study area region assign a per year fall rate for snags ranging from a rate of 0.065/year for smaller snags to 0.01/year for larger snags in their simulation modeling of stand dynamics incorporating wildfires and prescribed fire events (Reinhardt & Crookston, 2003). While the large snags included in our study are more likely to persist on the landscape than smaller snags, predictive performance may still have been impacted by snag falls during the lidar and field data collection time lag.

The probability of occurrence maps created for our snag classes and shrub cover thresholds allow for some prioritizing of error structures and adaptations for particular project needs. For example, if the goal is to map all areas that could potentially contain a large snag with little probability of missing a large snag, then shifting the threshold to minimize false negative (omission) errors may be the best approach. Alternatively, when the purpose is to highlight patches for conservation purposes with the high likelihood of containing large snags, maps using a threshold that minimizes false positive errors would be more

appropriate. Decisions such as the optimal threshold methods for the probability of occurrence predictive maps and the amount of error acceptable for a particular application bring up an important point in the secondary use of mapping products for management or research purposes: communication. The creators of map products are intimate with the map limitations and intended applications, as well as tradeoffs in errors. Communicating these limitations to secondary users is crucial in ensuring mapping products are utilized appropriately and that results and limitations are interpreted correctly. Feedback from users also helps to improve future mapping products and technology.

## 5. Conclusion

Our models for snag size classes and shrub distributions fall in the acceptable predictive range for many applications according to AUC values, although project specifics will ultimately determine what level of error is acceptable for their goals. Our maps provide important spatial prediction information about local-scale components of habitat, demonstrating the potential of remote sensing datasets to map these components in a post-fire landscape at a resolution relevant to many habitat mapping applications. The fine resolutions of our maps provide flexibility in the species mapping applications and allow for the aggregating of presence/absence data to represent density measures of particular snag classes across larger areas (Vogeler, 2014). While our study area covered a range of forest vegetation zones along an elevation gradient, these models were still created in a single fire complex and post-fire time period. Future research should expand these efforts to additional fire complexes and along a post-fire chronosequence, as well as explore other spatial datasets that may improve prediction accuracies.

## Acknowledgments

Our research was funded by the National Aeronautics and Space Administration, Carbon Cycle Program (NASA Grant 10-CARBON10-45). We thank our field technicians for assisting in data collection and Keith Olsen for initial assistance in lidar processing methods.

## References

Agresti, A. (2007). *Categorical data analysis* (Second Edition ). Hoboken, NJ: Wiley-Interscience.

Bishop, B. D., Dietterick, B. C., White, R. A., & Mastin, T. B. (2014). Classification of plot-level fire-caused tree mortality in a redwood forest using digital orthophotography and LiDAR. *Remote Sensing*, *6*, 1954–1972.

Burnham, K. P., & Anderson, D. R. (2002). *Model selection and multimodel inference: A practical information-theoretic approach*. Springer Science & Business Media (Chapter 2).

Crist, E. P. (1985). A TM tasseled cap equivalent transformation for reflectance factor data. *Remote Sensing of Environment*, *17*, 301–306.

Dale, V. H., Joyce, L. A., Mcnulty, S., Neilson, R. P., Ayres, M. P., Flannigan, M. D., Hanson, P. J., Irland, L. C., Lugo, A. E., Peterson, C. J., Simberloff, D., Swanson, F. J., Stocks, B. J., & Wotton, B. M. (2001). Climate change and forest disturbances: Climate change can affect forests by altering the frequency, intensity, duration, and timing of fire, drought, introduced species, insect and pathogen outbreaks, hurricanes, windstorms, ice storms, or landslides. *BioScience*, *51*, 723.

Dalponte, M. (2008). Fusion of hyperspectral and LIDAR remote sensing data for classification of complex forest areas. *Geoscience and Remote Sensing*, *46*, 1416–1427.

Davis, R. J., Dugger, K. M., Mohoric, S., Evers, L., & Aney, W. C. (2011). Northwest forest plan—The first 15 years (1994–2008): Status and trends of northern spotted owl populations and habitats. *General Technical Report PNW-GTR-850* (147 pp.).

Eidenshink, J., Schwind, B., Brewer, K., Zhu, Z. L., Quayle, B., & Howard, S. (2007). A project for monitoring trends in burn severity. *Fire Ecology*, *3*, 3–21.

Eklund, A., Wing, M. G., & Sessions, J. (2009). Evaluating economic and wildlife habitat burned landscapes. *Western Journal of Applied Forestry*, *24*, 67–75.

Escuin, S., Navarro, R., & Fernández, P. (2008). Fire severity assessment by using NBR (Normalized Burn Ratio) and NDVI (Normalized Difference Vegetation Index) derived from LANDSAT TM/ETM images. *International Journal of Remote Sensing*, *29*, 1053–1073.

Eskelson, B. N. I., Temesgen, H., & Hagar, J. C. (2012). A comparison of selected parametric and imputation methods for estimating snag density and snag quality attributes. *Forest Ecology and Management*, *272*, 26–34.

Everett, R., Lehmkuhl, J., Schellhaas, R., Ohlson, P., Keenum, D., Riesterer, H., & Spurbeck, D. (2000). Snag dynamics in a chronosequence of 26 wildfires on the east slope of the Cascade Range in Washington State, USA. *International Journal of Wildland Fire*, *9*, 223–234.

Freeman, E. A., & Moisen, G. (2008). PresenceAbsence: An R package for presence-absence model analysis. *Journal of Statistical Software*, *23*(11), 1–31 (http://www.jstatsoft.org/v23/i11 Paper URL: http://cran.r-project.org/web/packages/PresenceAbsence/index.html).

Goetz, S. J., Steinberg, D., Betts, M. G., Holmes, R. T., Doran, P. J., Dubayah, R., & Hofton, M. (2010). Lidar remote sensing variables predict breeding habitat of a Neotropical migrant bird. *Ecology*, *91*, 1569–1576.

Guisan, A., & Zimmermann, N. E. (2000). Predictive habitat distribution models in ecology. *Ecological Modelling*, *135*, 147–186.

Haggard, M., & Gaines, W. L. (2001). Effects of stand-replacement fire and salvage logging on a cavity-nesting bird community in eastern Cascades, Washington. *Northwest Science*, *75*, 387–396.

Hudak, A. T., Crookston, N. L., Evans, J. S., Falkowski, M. J., Smith, A. M., Gessler, P. E., & Morgan, P. (2006). Regression modeling and mapping of coniferous forest basal area and tree density from discrete-return lidar and multispectral satellite data. *Canadian Journal of Remote Sensing*, *32*(2), 126–138.

Larson, A. J., & Franklin, J. F. (2005). Patterns of conifer tree regeneration following an autumn wildfire event in the western Oregon Cascade Range, USA. *Forest Ecology and Management*, *218*, 25–36.

Lefsky, M. A., Cohen, W. B., Parker, G. G., & Harding, D. J. (2002). Lidar remote sensing for ecosystem studies lidar, an emerging remote sensing technology that directly measures the three-dimensional distribution of plant canopies, can accurately estimate vegetation structural attributes and should be of particular interest to forest, landscape, and global ecologists. *BioScience*, *52*, 19–30.

Lentile, L. B., Holden, Z. A., Smith, A. M. S., Falkowski, M. J., Hudak, A. T., Morgan, P., Lewis, S. A., Gessler, P. E., & Benson, N. C. (2006). Remote sensing techniques to assess active fire characteristics and post-fire effects. *International Journal of Wildland Fire*, *15*, 319–345.

Lumley, T. (2013). Package 'leaps'. http://cran.r-project.org/web/packages/leaps/ leaps.pdf

MacKenzie, D. I. (Ed.). (2006). *Occupancy estimation and modeling: Inferring patterns and dynamics of species occurrence*. Academic Press (Chapter 3).

Martin, K., & Eadie, J. M. (1999). Nest webs: A community-wide approach to the management and conservation of cavity-nesting forest birds. *Forest Ecology and Management*, *115*, 243–257.

Martinuzzi, S., Vierling, L. A., Gould, W. A., Falkowski, M. J., Evans, J. S., Hudak, A. T., & Vierling, K. T. (2009). Mapping snags and understory shrubs for a LiDAR-based assessment of wildlife habitat suitability. *Remote Sensing of Environment*, *113*, 2533–2546.

McGaughey, R. J. (2009). *FUSION/LDV: Software for LIDAR data analysis and visualization*. Seattle, WA, USA: US Department of Agriculture, Forest Service, Pacific Northwest Research Station, 123.

McPherson, J. M., Jetz, W., & Rogers, D. J. (2004). The effects of species' range sizes on the accuracy of distribution models: Ecological phenomenon or statistical artifact? *Journal of Applied Ecology*, *41*, 811–823.

Mutlu, M., Popescu, S. C., Stripling, C., & Spencer, T. (2008). Mapping surface fuel models using lidar and multispectral data fusion for fire behavior. *Remote Sensing of Environment*, *112*, 274–285.

Nappi, A., & Drapeau, P. (2011). Pre-fire forest conditions and fire severity as determinants of the quality of burned forests for deadwood-dependent species: The case of the black-backed woodpecker. *Canadian Journal of Forest Research*, *41*, 994–1003.

Nappi, A., Drapeau, P., & Savard, J. P. L. (2004). Salvage logging after wildfire in the boreal forest: Is it becoming a hot issue for wildlife? *The Forestry Chronicle*, *80*, 67–74.

Pearce, J., & Ferrier, S. (2000). *Evaluating the predictive performance of habitat models developed using logistic regression*, *133*. (pp. 225–245), 225–245.

Pflugmacher, D., Cohen, W. B., & Kennedy, R. E. (2012). Using Landsat-derived disturbance history (1972–2010) to predict current forest structure. *Remote Sensing of Environment*, *122*, 146–165.

Pflugmacher, D., Cohen, W. B., Kennedy, R. E., & Yang, Z. (2014). Using Landsat-derived disturbance and recovery history and lidar to map forest biomass dynamics. *Remote Sensing of Environment*, *151*, 124–137.

R Development Core Team (2014). *R: A language and environment for statistical computing*. Vienna, Austria: R Foundation for Statistical Computing.

Radeloff, V. C., Hammer, R. B., Stewart, S. I., Fried, J. S., Holcomb, S. S., & McKeefry, J. F. (2005). The wildland-urban interface in the United States. *Ecological Applications*, *15*, 799–805.

Reinhardt, E., & Crookston, N. L. (Technical Editors). (2003). The Fire and Fuels Extension to the Forest Vegetation Simulator. Gen. Tech. Rep. RMRS-GTR-116. Ogden, UT: U.S. Department of Agriculture, Forest Service, Rocky Mountain Research Station. 209 p.

Ruiz-Gazen, A., & Villa, N. (2008). *Storms prediction: Logistic regression vs random forest for unbalanced data*. arXiv (preprint arXiv:0804.0650).

Saab, V. A., Dudley, J., & Thompson, W. L. (2004). Factors influencing occupancy of nest cavities in recently burned forests factors influencing occupancy of nest cavities. *The Condor*, *106*, 20–36.

Sousa, P. J. (1983). Habitat suitability index models: Lewis' woodpecker (No. FWS/OBS-82/10.32). ish and Wildlife Service Fort Collins Co Western Energy And Land Use Team.

Vierling, K. T., Swift, C. E., Hudak, A. T., Vogeler, J. C., & Vierling, L. A. (2014). How much does the time lag between wildlife field-data collection and LiDAR-data acquisition

matter for studies of animal distributions? A case study using bird communities. *Geoscience and Remote Sensing*, *5*, 185–193.

Vogeler, J. C. (2014). *The use of remote sensing for characterizing forests in wildlife habitat modeling.* (Dissertation) Corvallis, Oregon: Department of Forest Ecosystems and Society, Oregon State University.

Weber, M. G., & Flannigan, M. D. (1997). Canadian boreal forest ecosystem structure and function in a changing climate: impact on fire regimes. *Environmental Reviews*, *5*, 145–166.

Wing, M. G., Eklund, A., & Sessions, J. (2010). Applying LiDAR technology for tree measurements in burned landscapes. *International Journal of Wildland Fire*, *19*, 104–114.

Wing, B. M., Ritchie, M. W., Boston, K., Cohen, W. B., & Olsen, M. J. (2015). Individual snag detection using neighborhood attribute filtered airborne lidar data. *Remote Sensing of Environment*, *163*, 165–179.

Wulder, M. A., White, J. C., Alvarez, F., Han, T., Rogan, J., & Hawkes, B. (2009). Characterizing boreal forest wildfire with multi-temporal Landsat and LIDAR data. *Remote Sensing of Environment*, *113*, 1540–1555.